Research in Astronomy and Astrophysics, 23:065018 (9pp), 2023 June https://doi.org/10.1088/1674-4527/accb7a

The Year-scale X-Ray Variations in the Core of M87

Yu-Lin Cheng[1], Fei Xiang[1,5], Heng Yu[2], Shu-Mei Jia[3], Xiang-Hua Li[1], Cheng-Kui Li[3], Yong Chen[3], and Wen-Cheng Feng[4]
[1] Department of Astronomy, Yunnan University, Kunming 650091, China; chengyl@mail.ynu.edu.cn, xhli@ynu.edu.cn
[2] Department of Astronomy, Beijing Normal University, Beijing 100875, China
[3] Key Laboratory of Particle Astrophysics, Institute of High Energy Physics, Chinese Academy of Sciences, Beijing 100049, China
[4] Department of Physics and Institute of Theoretical Physics, Nanjing Normal University, Nanjing 210023, China
Received 2022 December 6; revised 2023 March 15; accepted 2023 March 21; published 2023 May 30

Abstract

The analysis of light variation of M87 can help us understand the disk evolution. In the past decade, M87 has experienced several short-term light variabilities related to flares. We also find that there are year-scale X-ray variations in the core of M87. Their light variability properties are similar to clumpy-ADAF. By re-analyzing 56 Chandra observations from 2007 to 2019, we distinguish the "non-flaring state" from "flaring state" in the light variability. After removing flaring state data, we identify four gas clumps in the nucleus and all of them can be well fitted by the clumpy-ADAF model. The average mass accretion rate is $\sim 0.16 M_{\odot}\,\mathrm{yr}^{-1}$. We analyze the photon index (Γ)–flux (2–10 keV) correlation between the non-flaring state and flaring state. For the non-flaring states, the flux is inversely proportional to the photon index. For the flaring states, we find no obvious correlation between the two parameters. In addition, we find that the flare always occurs at a high mass accretion rate, and after the luminosity of the flare reaches the peak, it will be accompanied by a sudden decrease in luminosity. Our results can be explained as that the energy released by magnetic reconnection destroys the structure of the accretion disk, thus the luminosity decreases rapidly and returns to normal levels thereafter.

Key words: X-rays: galaxies – galaxies: clusters: individual (M87) – accretion – accretion disks

1. Introduction

M87 (NGC 4486) is a large radio galaxy located in the Virgo Cluster (Macchetto et al. 1997) at a distance of 18.5 Mpc from us (Blakeslee et al. 2001). Its central "engine" is a supermassive black hole with a mass of about $6.5 \times 10^9 M_{\odot}$ (Event Horizon Telescope Collaboration et al. 2019). M87 emits a high-energy plasma jet extending about 5000 lt-yr from the core, and its relativistic jet is misaligned by an angle of $\sim 30°$ with respect to our line of sight (Bicknell & Begelman 1996). The jet components of M87 can be resolved in radio, optical/UV and X-ray bands. Considering its large inclination, it is an ideal case to study the accretion disk of black hole and the details near the jet.

The radiation mechanism of M87 has been discussed by many researchers. Wilson & Yang (2002) assumed that the X-ray radiation came from the standard thin disk. With a canonical radiation efficiency ~ 0.1 (Di Matteo et al. 2000), the predicted nuclear luminosity of M87 should be $\sim 5 \times 10^{44}\,\mathrm{erg\,s^{-1}}$ (Di Matteo et al. 2003). However, the luminosity observed by Chandra is $\sim 7 \times 10^{40}\,\mathrm{erg\,s^{-1}}$ (Di Matteo et al. 2003). It means that the actual radiation efficiency is $\sim 10^{-5}$, four orders magnitude lower than the canonical value, and the required value of radiation efficiency was consistent with the prediction of the Advection Dominated Accretion Flow (ADAF, Narayan & Yi 1995) models. Di Matteo et al. (2003) fitted the X-ray spectra of M87 with ADAF models and verified that its X-ray radiation was dominated by ADAF.

As a Low Luminosity AGN (LLAGN, Yuan & Narayan 2014), M87 does not have strong flux like blazars. However, from the past observations, it was found that M87 has experienced several short-term light variabilities. In 2005, H.E.S.S. captured a TeV emission of M87 with timescales of a few days (Aharonian et al. 2006). The joint observation of Chandra found a giant flare (Harris et al. 2006) accompanied by this TeV event in knot HST-1 (0.″86 away from the core). Therefore, Cheung & Stawarz (2007) proposed HST-1 as a candidate for TeV emission. However, another TeV flare was observed by H.E.S.S., MAGIC (Albert et al. 2008) and VERITAS (Acciari et al. 2008) in 2008 which lasted for about two weeks. In the following days, Chandra observations suggested that the X-ray intensity of the nucleus was 2–3 times higher than usual (Harris & Cheung 2009). Different to the first outburst, HST-1 was in a low state at this time and its X-ray flux was lower than that in the nucleus. In 2010, a third VHE γ-ray burst was captured and the timescale of intensity-doubling was day-scale (Aliu et al. 2012). After the TeV emission, X-ray intensity in the nucleus was also enhanced. Therefore, it can be confirmed that the site of the TeV flare is the nucleus rather

[5] This paper is dedicated to the memory of my wonderful tutor Fei Xiang, who recently passed away.

than HST-1 (Harris et al. 2011). It is still unclear where the X-ray flare originates. Similar to the solar flare, the X-ray flares of M87 may be triggered by magnetic reconnection (Yuan et al. 2009; Aschwanden 2011; Yang et al. 2019) or from the mini-jet (Giannios et al. 2009). For the intraday variability of the M87 core in 2017, Imazawa et al. (2021) suggested that the emission might come from the inverse Compton scattering in the jet.

Previous studies mainly focused on these striking flare events in the day-scale or month-scale, but the research on the year-scale light variability of M87 was rare. For LLAGNs, the emission of year-scale variation is considered to be related to the accretion mode of the disk. Wang et al. (2012) proposed that the inhomogeneous accretion flow in LLAGNs might be clumpy (i.e., clumpy-ADAF), which originated from the thermal instability in the accretion flow or is affected by gravity. Once the clump is formed, it will fall toward the center of the black hole under the tidal force and bring about a long-term light variation. By re-analyzing Chandra observations from 2007 to 2008, Xiang & Cheng (2020) found a year-scale X-ray variation in the core of M87, and successfully fitted the spectra with a simple clumpy accretion model.

To validate the clumpy-ADAF model, we check the M87 observations of Chandra from 2007 to 2019 and obtain the long-term X-ray variation of M87. We distinguish the "non-flaring state" from "flaring state" in the light curve with a universal classification method. Based on the work of Xiang & Cheng (2020), we find another three year-scale variability components and reproduce them with a clumpy accretion model. This paper is developed as follows: the Chandra data analysis is described in Section 2, the clumpy accretion model fitting results are presented in Section 3, we discuss the physical characteristics of the clump in Section 4 and finally, conclusions are listed in Section 5. The distance r of M87 used in this study is 18.5 Mpc.

2. Data and Analysis

To study the long-term X-ray variation of M87, we select the data of M87 observed by Chandra X-Ray Observatory with subarcsecond resolution. From 2007 July 31 to 2019 March 28, 56 observations are carried out using the Advanced CCD Imaging Spectrometer (ACIS) and back-illuminated S3 detector. The time period of each observation is about 4.7 ks and the observation mode is FAINT. A 0.4 s frame time is set to minimize the significant pileup effect (Harris et al. 2006). We use CIAO (version 4.13) to analyze the Chandra data retrieved from the archive. First of all, we reprocess the data by the `chandra_repro` script to ensure that the latest calibrations is consistent with the current version of CIAO.

As the core is very close to HST-1, only $0\farcs86$, sometimes the two regions cannot be well distinguished. When HST-1 is bright, possible "light pollution" from HST-1 might happen in the nucleus region, especially for the outburst event of HST-1 in 2005 (Harris & Cheung 2009; Harris et al. 2011). Xiang & Cheng (2020) analysis showed the nucleus region is little influenced by HST-1 from 2007 to 2008. In 2008, the nucleus was brighter than HST-1, and then the luminosity of HST-1 continued to decrease. Therefore, the "light pollution" of HST-1 on the nucleus can be ignored in our analysis, but we are still careful for border of the core region which might influence the result of our spectra analysis. We adopt a box region with a size of $0\farcs8 \times 2\farcs6$ including nucleus (Yang et al. 2019). Since the core is spherical, we take the brightest center of the core as the center of the box region (shown in the top panel of Figure 1).

The surface of ACIS has accumulated a layer of contamination over the mission (Plucinsky et al. 2018). Since our data span 12 yr, we check the stability of the instrument during this long-term observation. We take a rectangular region with a size of $17'' \times 8\farcs5$ without resolved point sources as the background region, whose center is located at R.A. $= 12^{\rm h}30^{\rm m}49\fs25$, decl. $= 12°23'19\farcs10$ (J2000) (shown in the top panel of Figure 1). The photon count rate of the background region of all observations between 2.0 and 10.0 keV are nearly stable as shown in the bottom panel of Figure 1. Their average value is about 0.023 ± 0.002 cts s^{-1} (the red line in the bottom panel of Figure 1). Thus we omit the instrument contamination at hard X-ray band of 2.0–10.0 keV.

3. Results

3.1. Energy Spectra Fitting

The X-ray from jet features of M87 is supposed to come from synchrotron emission and can be characterized by a power law (Harris & Krawczynski 2002; Wilson & Yang 2002; Harris et al. 2003). In XSPEC (version 12.1.1), we use a power-law model with Galactic absorption to fit the nuclear X-ray spectra (Arnaud 1996; Xiang & Cheng 2020):

$$\text{Model} = \text{Wabs} * \text{Powerlaw}. \quad (1)$$

The column density of hydrogen ($n_{\rm H}$) is fixed as 6.1×10^{20} cm^{-2} (Wilson & Yang 2002; Xiang & Cheng 2020). We obtained photon index (Γ), normalization of power-law and flux in 2.0–10.0 keV and the results are listed in Table 1. All the reduced chi-squares are less than 1.20 which indicates that our spectra fitting results are reliable. The long-term X-ray light curve of the core is shown in Figure 2. The variation of the flux intensity is similar to the light curve in previous works (Harris & Cheung 2009; MAGIC Collaboration et al. 2020).

3.2. Clumpy Accretion Model Fitting

It can be clearly seen from the M87 black hole image published by the Event Horizon Telescope (EHT) in 2017 that the bright ring morphology appears to be inhomogeneous (EHT MWL Science Working Group et al. 2021). Meanwhile, the year-scale variation of M87 is a long-term evolution process,

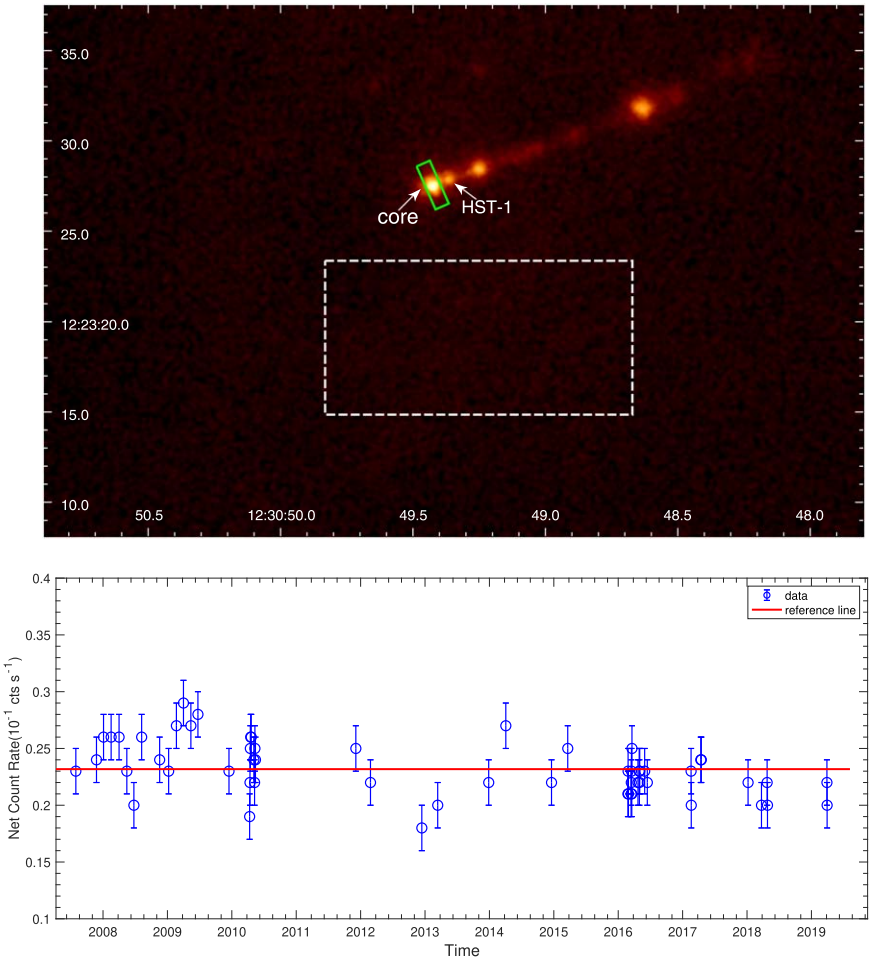

Figure 1. (Top) The X-ray image of M87 observed by Chandra on 2016 February 24 (obsID 18 781). The images are binned on a scale of 1/8 native ACIS pixel and then smoothed with a Gaussian of FWHM $= 0\farcs5$. The box in green solid line is the selected source region for the core, and the rectangle in white dotted line is the background region. (Bottom) The variation of photon count rate of background region over time of all observations. The solid red line represents the average value.

and the light variability characteristics are similar to the clumpy-ADAF model proposed by Wang et al. (2012). The accretion rates can be written in Eddington units, $\dot{M} = \dot{m}\dot{M}_{\rm Edd}$, where $\dot{M}_{\rm Edd}$ is the Eddington accretion rates which can be defined as: $\dot{M}_{\rm Edd} = L_{\rm Edd}/\eta c^2 = 2.2 \times 10^{-8} m\ M_\odot\ {\rm yr}^{-1}$ (Di Matteo et al. 2003), $m = M_{\rm BH}/M_\odot$ is the dimensionless mass of black hole, c is the light speed, η is the X-ray radiation efficiency ($\eta = 0.1$ for standard models), $L_{\rm Edd}$ is the Eddington luminosity. $\dot{m}$ can be expressed as $L/L_{\rm Edd}$. $L_{\rm Edd} = 1.25 \times 10^{38} m\,{\rm erg\,s^{-1}}$ when $\eta = 0.1$ (Wang et al. 2012). In M87 hot accretion flow, η is about 10^{-5} (Di Matteo et al. 2003). The luminosity of black hole is $L = 4\pi r^2 F\,{\rm erg\,s^{-1}}$, where F is flux, r is the distance of M87. Then we can obtain the mass accretion rate of M87 as:

$$\dot{M} = \frac{L}{L_{\rm Edd}} \times \frac{\eta_{10^{-5}}}{\eta_{0.1}} \times \dot{M}_{\rm Edd}, \tag{2}$$

where $\eta_{0.1} = \eta/0.1$ and $\eta_{10^{-5}} = \eta/10^{-5}$. With this formula, we find that the X-ray luminosity is in proportion to the mass accretion rate which is also mentioned by Ishibashi & Courvoisier (2009).

In the past, both theory and observation supported that the accretion flow around black hole in LLAGNs was inhomogeneous (Celotti & Rees 1999). Due to thermal instability and viscous instability, it would create cold clumps in the disk (Krolik 1998) and then fallback into the central black hole. During the process of accretion, the clump will be disrupted by tidal force and release a burst of energy (Celotti & Rees 1999; Strubbe & Quataert 2009). As for the mass accretion rate of clumpy gas, Xiang & Cheng (2020) derived a solution as follows:

$$\dot{M}(x,\tau) = \dot{M}_0 \left(\frac{1}{2x} - \frac{2x}{\tau}\right) \frac{x^{3/4}}{\tau} e^{-\frac{1+x^2}{\tau}} I_{1/4}\left(\frac{2x}{\tau}\right), \tag{3}$$

Table 1
List of the Spectra Fitting Results of the Core

obsID	Time (MJD)	Photon Index	Norm (10^{-5})	flux$_{2-10\ \mathrm{KeV}}$ (10^{-12} erg s^{-1} cm^{-2})	χ^2/DOF
7354	54,312	2.27 ± 0.06	78 ± 3	1.36 ± 0.11	22.39/39
8575	54,429	2.10 ± 0.05	130 ± 4	2.88 ± 0.17	107.06/108
8576	54,469	2.11 ± 0.05	14 ± 4	3.06 ± 0.20	27.16/33
8577	54,512	1.76 ± 0.03	216 ± 5	8.02 ± 0.36	58.36/56
8578	54,557	1.72 ± 0.05	126 ± 4	4.96 ± 0.26	43.42/47
8579	54,601	2.16 ± 0.05	121 ± 4	2.46 ± 0.16	122.41/106
8580	54,641	1.72 ± 0.04	163 ± 4	6.41 ± 0.33	49.67/46
8581	54,685	2.04 ± 0.06	84 ± 3	2.02 ± 0.14	94.01/79
10282	54,787	2.18 ± 0.06	85 ± 3	1.66 ± 0.15	53.60/77
10283	54,838	2.21 ± 0.06	99 ± 3	1.84 ± 0.16	89.28/88
10284	54,882	2.24 ± 0.06	97 ± 3	1.76 ± 0.14	14.14/23
10285	54,922	2.06 ± 0.06	89 ± 3	2.10 ± 0.17	18.58/22
10286	54,964	2.18 ± 0.06	108 ± 4	2.11 ± 0.13	108.54/91
10287	55,004	2.12 ± 0.04	117 ± 4	2.48 ± 0.17	82.84/103
10288	55,180	2.07 ± 0.05	143 ± 5	3.14 ± 0.18	38.38/34
11512	55,297	2.03 ± 0.04	231 ± 5	5.65 ± 0.25	99.46/105
11513	55,299	2.30 ± 0.05	164 ± 4	2.71 ± 0.19	42.37/38
11514	55,301	2.04 ± 0.06	118 ± 4	2.82 ± 0.21	32.45/28
11515	55,303	2.19 ± 0.05	136 ± 4	2.63 ± 0.20	55.49/55
11516	55,306	2.06 ± 0.05	115 ± 4	2.70 ± 0.19	46.57/55
11517	55,321	2.25 ± 0.05	161 ± 4	2.83 ± 0.17	32.93/38
11518	55,325	2.26 ± 0.06	117 ± 4	2.04 ± 0.16	108.11/92
11519	55,327	2.23 ± 0.06	109 ± 3	2.00 ± 0.15	79.73/89
11520	55,330	2.19 ± 0.06	101 ± 3	1.94 ± 0.14	81.00/86
13964	55,899	2.16 ± 0.06	120 ± 4	2.41 ± 0.18	23.70/26
13965	55,982	2.14 ± 0.06	107 ± 4	2.23 ± 0.17	79.64/86
14974	56,273	2.20 ± 0.06	100 ± 4	1.93 ± 0.13	82.19/76
14973	56,363	2.19 ± 0.06	105 ± 4	2.03 ± 0.21	62.64/79
16042	56,652	2.15 ± 0.08	71 ± 3	1.45 ± 0.14	51.79/55
16043	56,749	2.09 ± 0.06	113 ± 4	2.53 ± 0.19	74.20/88
17056	57,008	2.25 ± 0.08	103 ± 4	1.83 ± 0.16	19.63/18
17057	57,100	1.97 ± 0.07	105 ± 5	2.90 ± 0.23	17.31/16
18233	57,441	2.26 ± 0.03	59 ± 1	1.03 ± 0.03	129.62/124
18781	57,442	2.22 ± 0.03	60 ± 3	1.12 ± 0.04	84.04/77
18782	57,444	2.23 ± 0.03	62 ± 1	1.13 ± 0.05	55.06/66
18809	57,459	2.24 ± 0.10	58 ± 4	1.05 ± 0.14	34.69/39
18810	57,460	2.26 ± 0.11	61 ± 4	1.07 ± 0.13	30.13/39
18811	57,461	2.31 ± 0.10	61 ± 4	0.99 ± 0.11	35.67/39
18812	57,463	2.26 ± 0.10	59 ± 4	1.04 ± 0.13	39.33/41
18813	57,464	2.18 ± 0.09	61 ± 4	1.18 ± 0.13	30.50/41
18783	57,498	2.33 ± 0.04	52 ± 1	0.83 ± 0.03	117.91/108
18232	57,505	2.18 ± 0.04	63 ± 2	1.24 ± 0.06	78.34/76
18836	57,506	2.18 ± 0.03	64 ± 1	1.25 ± 0.04	133.45/134
18837	57,508	2.38 ± 0.06	55 ± 2	0.80 ± 0.06	47.90/47
18838	57,536	2.35 ± 0.03	51 ± 1	0.79 ± 0.03	160.11/137
18856	57,551	2.36 ± 0.05	49 ± 1	0.74 ± 0.04	149.33/124
19457	57,799	2.23 ± 0.08	83 ± 4	1.37 ± 0.14	58.57/52
19458	57,800	2.22 ± 0.11	66 ± 4	1.23 ± 0.14	41.37/43
20034	57,854	1.97 ± 0.04	115 ± 3	3.10 ± 0.13	95.16/102
20035	57,857	2.10 ± 0.04	103 ± 3	2.26 ± 0.11	91.83/84
20488	58,122	1.97 ± 0.07	131 ± 7	3.59 ± 0.24	40.20/41
20489	58,198	2.01 ± 0.07	113 ± 2	3.01 ± 0.23	72.90/69
21075	58,230	1.98 ± 0.04	175 ± 5	4.59 ± 0.20	85.46/101
21076	58,232	2.00 ± 0.04	190 ± 5	4.93 ± 0.21	118.29/103
21457	58,569	2.13 ± 0.05	83 ± 3	1.75 ± 0.09	144.15/123
21458	58,570	2.16 ± 0.05	88 ± 3	1.76 ± 0.10	119.93/117

Note. The flux is in 2.0–10.0 keV and the errors of those parameters are calculated with the confidence of 68%. From 2007 July 31 to 2019 March 28, 56 observations are carried out via Chandra/ACIS.

and

$$\tau = (t - t_0)/\tau_0, \tag{4}$$

where $\dot{M}_0 = 6\pi\nu\Sigma_0$, Σ_0 is the initial surface density of the clumpy gas (Xiang & Cheng 2020), ν is kinematic viscosity parameter (Lin & Schwartz 1987), x can be written in R/R_0 and represents the dimensionless distance to central BH and R_0 is the radius where the clump forms, R_0 is about $100R_{\mathrm{Sch}} \sim 1000R_{\mathrm{Sch}}$ (Wang et al. 2012), t_0 stands for the start date of the clumpy accretion, τ_0 is the timescale of gas falling and $I_{1/4}$ is the modified Bessel function.

From 2007 to 2008 data, Xiang & Cheng (2020) found there was an obvious anti-correlation between photon index and flux. Based on this characteristic, Xiang & Cheng (2020) divided the states of nucleus into two types and those five points with lower flux and higher index were defined as the "first class;" three points with higher flux and lower index were defined as the "second class." The first class of the low state was corresponding to the pure ADAF model (Li et al. 2009) and had been successfully fitted by the clumpy accretion model (Xiang & Cheng 2020). The second class of the high state could be separated into two components, an ADAF component and a flaring component, and the former might also match the value of disk evolution. However, this classification method cannot work well for the long-term light curve. It can be seen from the right panel of Figure 2 that there is no obvious bimodal structure in the histogram distribution of photon index and flux in the 12 yr observations. In order to obtain the year-scale variation in the light curve, we propose a universal classification method for these two states. The specific classification steps are as follows:

Select all points within a half year period around each point. If there are no points in the range, select the two nearest points on the left and right. We check whether this point is the maximum value in this range and is 50% higher than the average value of the rest points. For points satisfying the condition, it is considered to be at the flaring state. After removing these points, this calculation process is repeated until there are no new flaring state points identified.

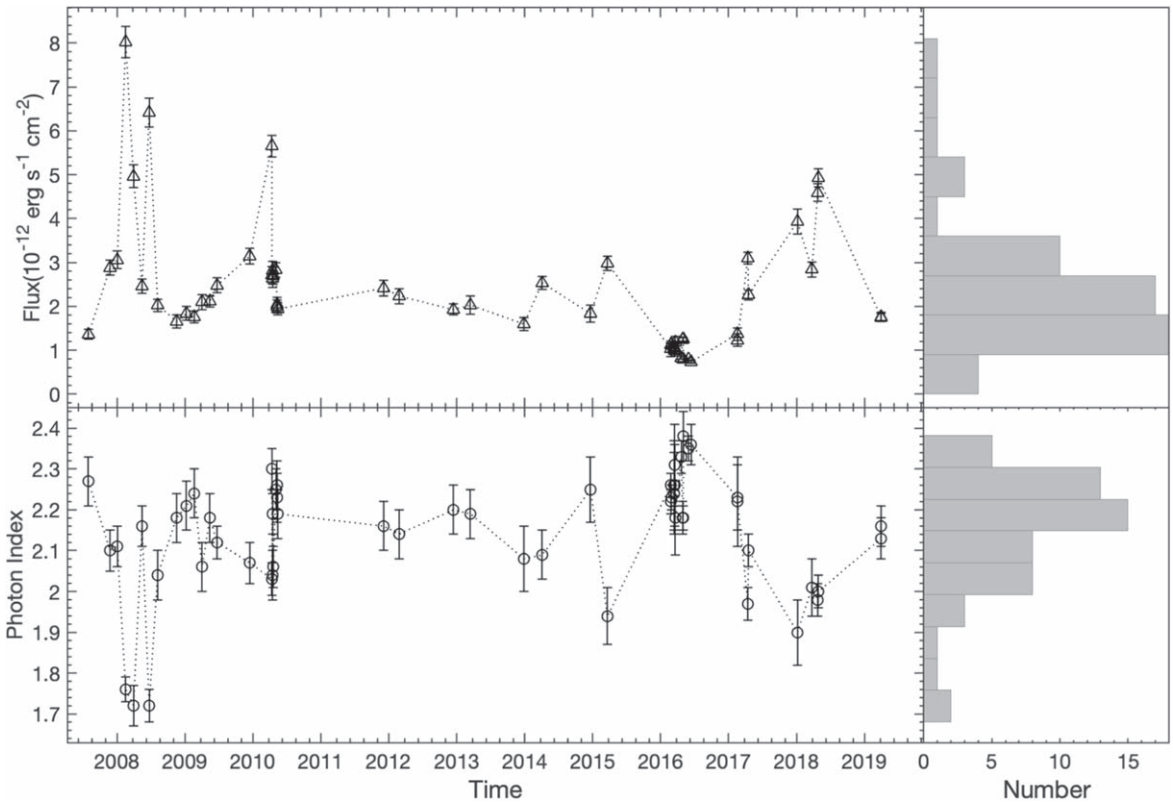

Figure 2. (Top left) The long-term X-ray light curve of M87 from 2007 to 2019. (Bottom left) The photon index of the core from the spectral fitting result corresponding to the above panel. The top right panel and the lower right panel are the histogram distribution of flux and photon index, respectively.

The results obtained by this method are shown in Figure 3. These blue triangle points are classified into the non-flaring state which are considered to be accompanied by the clumpy accretion activities. These points marked in magenta dots are at the flaring state which are related to the flare events. Meanwhile, the distinguished flaring state and non-flaring state from 2007 to 2008 are consistent with the classification results in Xiang & Cheng (2020).

To meet the conditions of the model fitting, it is necessary for us to divide the starting and ending time of the accretion process from the long-term observations. After excluding those flaring state points, we find that there are five local minima of brightness (segmented by the gray line in Figure 3). For the clumpy accretion model, the light curve will experience a rapid increase and then slow decrease during the accretion process (Wang et al. 2012). However, the decline rate after the flare event in 2010 April is much faster than the ascent rate of 2009, which is inconsistent with the physical characteristics described by the accretion model. Therefore, we do not take it as the beginning or end of the accretion process (the position is shown by gray dotted line in Figure 3). Based on this standard, four candidate clumpy accretion components are identified. The first component contains the entire time period of the accretion process in Xiang & Cheng (2020). Fitted these candidate accretion parts with formula (3), we get the results shown in Figure 4 and the fitting parameters are listed in Table 2. Meanwhile, we label the nine observations of flaring state with a sequence number.

4. Discussion

4.1. The Physical Characteristics of Clumpy Accretion

In Figure 4, it shows that those non-flaring state observations are basically on the fitting curve which illustrate that our classification method for clumpy accretion is reasonable. Although the luminosity dropped sharply to a very low state after the flare in 2010, it did not bring a great influence to the long-term evolution of the disk. We give a more detailed explanation of this phenomenon in Section 4.3.

Based on the parameters listed in Table 2, we can find that all of the dimensionless distance to central BH (x) are no more than 0.05, which indicates that the region where the clumps form is very close to the black hole. Our fitting results for the first clump are consistent with the results in Xiang & Cheng (2020). Although the size of the source region adopted in this paper ($0\farcs8 \times 2\farcs6$) is smaller than that in Xiang & Cheng (2020) ($1\farcs8 \times 2\farcs3$) which leads to higher luminosity and mass accretion rate, it does not change the position where the clump

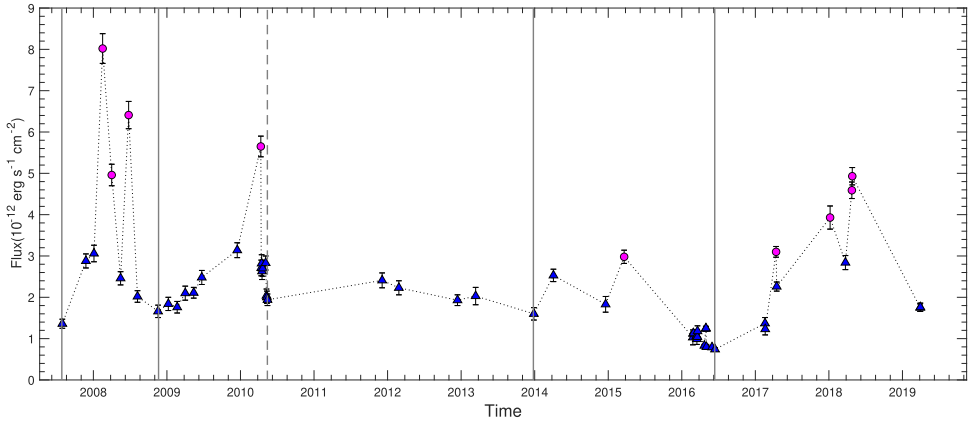

Figure 3. The light curve of the core. Blue triangles: the observations of the non-flaring state; magenta dots: the observations of the flaring state. The gray lines represent the position of the local minimum brightness.

forms. Meanwhile, it can be seen from Figure 4 that the accretion on the black hole is discontinuous and the size of the clump is randomly generated. Since the solution of the clumpy accretion is a function of mass accretion rate with time, the mass of the clump could be obtained through integration of $\dot{M}$ by time. When the mass accretion rate is lower than $0.1M_{\odot}\,\mathrm{yr}^{-1}$, the radiation generated by accretion is very weak. Therefore, we take $0.1M_{\odot}\,\mathrm{yr}^{-1}$ as the minimum threshold of the clumpy accretion. We define the time range above this threshold as the accretion timescale (ΔT) of a clumpy accretion. Based on this standard, we find that the accretion of the last gas clump had not been completed within the selected observation time range. According to the results predicted by the model, the accretion rate would drop to $0.1M_{\odot}\,\mathrm{yr}^{-1}$ on 2020 February 11. Then we obtain the mass of each clump by integral calculation. As the morphology of the clump is spherical, the radius of a clump could be estimated by $R_{\mathrm{c}} = (3M_{\mathrm{c}}/(4\pi n_{\mathrm{cl}}\, m_{\mathrm{p}}))^{\frac{1}{3}}$, where m_{p} is the mass of proton, n_{cl} is the density of gas clump and the typical density is $\sim 10^{14}\,\mathrm{cm}^{-3}$ (Xiang & Cheng 2020). The values of M_{c} and R_{c} are listed in Table 2, and the linear relationship between M_{c} and ΔT is given in Figure 5 (the dashed blue line). The regression equation is $M_{\mathrm{c}} = q_0 + q_1 \Delta T$ and their correlation coefficient is 0.98. The fitting parameter is $q_1 = 0.16 \pm 0.01$. From the linear fitting result, we can deduce that the timescale of clumpy accretion is determined by the size of the gas clump. With a mass of $\sim 0.16M_{\odot}$, the accretion process will last for about one year and lead to the variation of the X-ray luminosity.

4.2. The Γ–$\mathrm{F}_{2\text{–}10\ KeV}$ Correlation between Flaring State and Non-flaring State

The correlation between the photon index and flux in very-high-energy (VHE) gamma-rays of M87 have been discussed by Acciari et al. (2008). Due to the small number of observations, no obvious correlation was found. However, the long-term X-ray observations provides enough data for us to study the relationship between these two parameters. In order to test if there is any difference of the Γ–$F_{2\text{–}10\,\mathrm{keV}}$ distribution between the flaring state and non-flaring state, we take the photon index (Γ) and the flux of the two states, respectively. Then fitting these two parameters with a linear test function $\Gamma = p_0 + p_1\Phi_0$. The results are shown in Figure 6. The χ^2/dof of the linear fit of the non-flaring state is 43.68/45, with the parameter $p_1 = -0.10 \pm 0.01$; the χ^2/dof of the linear fit of the flaring state is 6.39/7, with the parameter $p_1 = -0.04 \pm 0.02$. However, as p_1 is consistent with zero, a constant photon index fit is applied to compare with the linear fitting results. The constant fit gave a χ^2/dof of 97.75/46 and 8.87/8 for the non-flaring state and flaring state, respectively. As a consequence, the fitting result shows that the flux is inversely proportional to the photon index for the non-flaring state (clumpy accretion components). For the flaring state (flare components), due to the χ^2/dof of the linear fit is consistent with the χ^2/dof of constant fit, no significant evidence is provided for the fact that there is any correlation between the two parameters.

The anti-correlation between photon index and flux in the X-ray band is also predicted by the ADAF model (Yuan et al. 2007). For LLAGNs, the X-ray emission is mainly dominated by the Comptonization of the hot gas in ADAF (Gu & Cao 2009; Xiang & Cheng 2020). However, according to the distribution of the two parameters, we can see that there is a cross connection between the non-flaring state and flaring state. For the flare in 2008, the peak flux reached 8.02×10^{-12} erg s^{-1} cm^{-2}, with the photon index of 1.76 (number 1 in Figures 4 and 6). Then the intensity dropped to 4.96×10^{-12} erg s^{-1} cm^{-2}, and the photon index was 1.72 (number 2 in Figures 4 and 6), almost the same as before. This shows that the event dominated by the flare varies greatly of the flux intensity, but keep the same feature of the photon index as the flare.

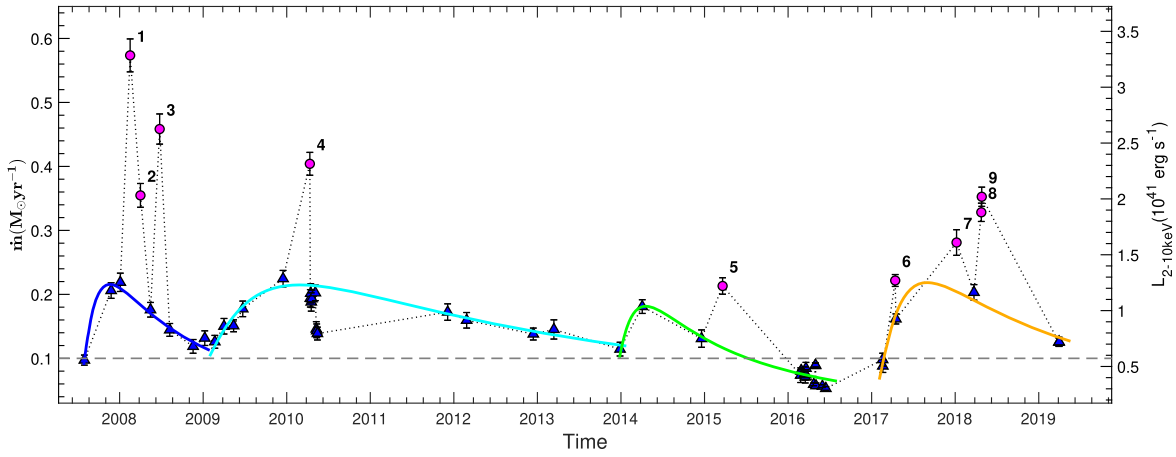

Figure 4. The long-term evolution of the mass accretion rate for the central BH of M87. Blue filled triangles: non-flaring state; magenta filled dots: flaring state. The solid lines represent the four clumpy accretion model fitting results. The gray dotted line represents the mass accretion rate of $0.1 M_\odot$ yr^{-1}.

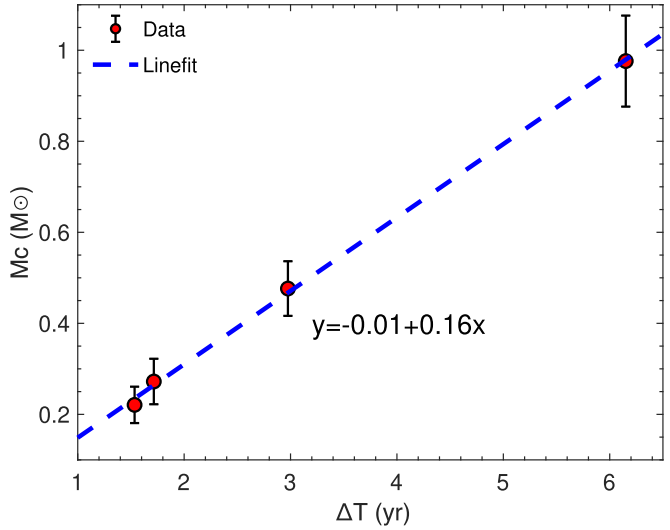

Figure 5. The variation of clump mass with accretion timescale. The red dot represents the mass of each clump; the dashed blue line is the linear fitting result. The error of the clump mass is calculated based on the 95% confidence limits of the model fitting result in Section 3.2.

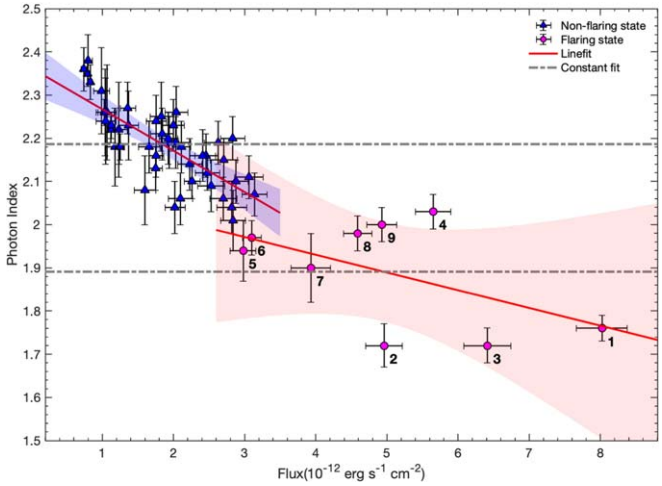

Figure 6. Distribution of photon index vs. flux. Blue triangles are the non-flaring state observations; magenta dots are the flaring state observations. The sequence numbers are corresponding to those in Figure 5. The dashed gray line represents a constant fit, and the red solid line represents a linear fit of the form $\Gamma = p_0 + p_1\Phi_0$, where Φ_0 is the spectral flux; the filled region represents the linear fit in 95% confidence limits. The value of p_1 is given in the text.

Table 2
The Parameters of the Clumpy Accretion Fitting Results

	$\dot{M}_0$ ($M_\odot$ yr^{-1})	x	τ_0 (days)	t_0 (date)	M_c ($M_\odot$)	R_c (10^{13} cm)
fit1	1.04	0.04	225	2007-05-23	0.23	8.62
fit2	1.03	0.02	819	2008-05-12	0.83	13.33
fit3	0.87	0.02	253	2013-09-27	0.30	9.45
fit4	1.05	0.03	387	2016-10-23	0.38	10.23

Note. M_c and R_c is the mass of gas clump and radius of clump, respectively. The mass of clump is the result of the integration of $\dot{M}$ by time.

Meanwhile, Γ–$F_{2-10\,\mathrm{keV}}$ distribution of the flaring states seems to present two branches. Such branches may imply different origin mechanisms of the flares. Carrying out high-frequency follow-up observation after the flare events may help us to understand the physical mechanism of this process.

4.3. Why can the Luminosity be Lower than the Clumpy Accretion Component?

It can be seen from the distribution of light curve in Figure 4 that the flare often occurs at a high mass accretion rate. After the intensity reaches the peak, a sudden decrease in luminosity

will be accompanied within a few days. The flare event in 2010 was particularly representative. The luminosity declined by 52.04% in two days after the peak intensity (number 4 in Figure 4). At this time, the luminosity was consistent with that of the non-flaring state. Then the luminosity decreased by 28.41% over the next 30 days. A light variability in 2017 is also very similar to this situation. We find that after the flare (number 6 in Figure 4), the luminosity decreased by 27.10% within three days which was consistent with the ADAF components. Due to the lack of observations afterwards, it cannot be sure whether the luminosity will continue to decrease for a period. But it is not a coincidence that the luminosity changes rapidly in a short time after the flare. Then, we analyze the origin mechanism of the flare and put forward a possible explanation for the above phenomenon.

The M87 image captured by EHT presents that the inhomogeneous ring-like structure seems to be clumpy. Meanwhile, the polarization map of M87 shows that there is strong magnetic field around the black hole (Event Horizon Telescope Collaboration et al. 2021a), which is closely related to the accretion mode of the black hole. Now it has been confirmed that the accretion flow in M87 is magnetically arrested disk (MAD, Xie & Zdziarski 2019; Event Horizon Telescope Collaboration et al. 2021b), and it is based on general relativistic magnetohydrodynamic simulations (GRMHD, McKinney et al. 2012; Yuan & Narayan 2014). In MHD model, there are magnetic arcades emerging from the disk into corona (Yuan et al. 2009). The formed flux ropes keep a balance between the magnetic compression and magnetic tension. Nevertheless, the equilibrium will be broken down by the turbulence in the photosphere and leads to rapid magnetic reconnection (Lin et al. 2003; Yuan et al. 2009). In this process, part of the energy transfers into the kinetic power of the plasma to ignite the flares, and part of it pushes the mass through the corona.

Our analysis shows that the flare might be triggered by magnetic reconnection, and the huge energy released from the process could blow material away from the accretion disk. As the structure of the accretion disk is destroyed, the luminosity decreases rapidly. However, with the accretion of the gas clump, the damaged part will be refilled. As a consequence, the luminosity returns to normal. This further shows that the flare does not have a great impact on the overall evolution of the accretion disk, which is consistent with the conclusion in Section 4.1.

5. Conclusions

We search the long-term X-ray variation of M87 from Chandra archival data. In our analysis, 56 observations from 2007 to 2019 are adopted. We distinguished the "non-flaring state" from "flaring state" with a universal classification method. The evolution of the non-flaring states could be well explained by the accretion of gas clumps. We also discussed the physical characteristics of clumpy accretion. The main results are listed as follows:

1. From 2007 to 2019, the central black hole of M87 have accreted four gas clumps. The timescale of accretion is determined by the size of the clump. Generally, it takes about one year to complete the accretion process of a mass of $\sim 0.16 M_{\odot}$.
2. We analyze the correlation of photon index against flux between the non-flaring state and flaring state. By linear fitting, we find that there is a significant anti-correlation between the two parameters of non-flaring states. However, the correlation is not significant for flaring states.
3. The flare always occurs at a high mass accretion rate. After the flare, there could be a steep luminosity drop to a level lower than that of the ADAF components. This hints that there might be a strong magnetic field around the black hole and flares could be related to the magnetic reconnections. The energy released by this process might temporarily destroy the structure of the disk. However, with the accretion of gas clumps, the damaged part could be filled again, and then the system returns to normal.

Acknowledgments

We thank the anonymous referee for detailed and constructive suggestions. This work is supported by the National Natural Science Foundation of China (Grant Nos. 11863006, U1838203, and U2038104), the Science & Technology Department of Yunnan Province—Yunnan University Joint Funding (2019FY003005), and the Bureau of International Cooperation, Chinese Academy of Sciences under the grant GJHZ1864. We thank Paolo Tozzi for his helpful comments.

ORCID iDs

Yu-Lin Cheng https://orcid.org/0000-0003-0239-4384
Heng Yu https://orcid.org/0000-0001-8051-1465

References

Acciari, V. A., Aliu, E., Beilicke, M., et al. 2008, ApJL, 684, L73
Aharonian, F., Akhperjanian, A. G., Bazer-Bachi, A. R., et al. 2006, Sci, 314, 1424
Albert, J., Aliu, E., Anderhub, H., et al. 2008, ApJL, 685, L23
Aliu, E., Arlen, T., Aune, T., et al. 2012, ApJ, 746, 141
Arnaud, K. A. 1996, in ASP Conf. Ser. 101, Astronomical Data Analysis Software and Systems V, ed. G. H. Jacoby & J. Barnes (San Francisco, CA: ASP), 17
Aschwanden, M. J. 2011, SoPh, 274, 119
Bicknell, G. V., & Begelman, M. C. 1996, ApJ, 467, 597
Blakeslee, J. P., Lucey, J. R., Barris, B. J., Hudson, M. J., & Tonry, J. L. 2001, MNRAS, 327, 1004
Celotti, A., & Rees, M. J. 1999, in ASP Conf. Ser. 161, High Energy Processes in Accreting Black Holes, ed. J. Poutanen & R. Svensson (San Francisco, CA: ASP), 325
Cheung, C. C., Harris, D. E., & Stawarz, Ł. 2007, ApJL, 663, L65

Di Matteo, T., Allen, S. W., Fabian, A. C., Wilson, A. S., & Young, A. J. 2003, ApJ, 582, 133
Di Matteo, T., Quataert, E., Allen, S. W., Narayan, R., & Fabian, A. C. 2000, MNRAS, 311, 507
EHT MWL Science Working Group, Algaba, J. C., Anczarski, J., et al. 2021, ApJL, 911, L11
Event Horizon Telescope Collaboration, Akiyama, K., Alberdi, A., et al. 2019, ApJL, 875, L6
Event Horizon Telescope Collaboration, Akiyama, K., Algaba, J. C., et al. 2021a, ApJL, 910, L12
Event Horizon Telescope Collaboration, Akiyama, K., Algaba, J. C., et al. 2021b, ApJL, 910, L13
Giannios, D., Uzdensky, D. A., & Begelman, M. C. 2009, MNRAS, 395, L29
Gu, M., & Cao, X. 2009, MNRAS, 399, 349
Harris, D. E., Biretta, J. A., Junor, W., et al. 2003, ApJL, 586, L41
Harris, D. E., Cheung, C. C., Biretta, J. A., et al. 2006, ApJ, 640, 211
Harris, D. E., Cheung, C. C., Stawarz, Ł., Biretta, J. A., & Perlman, E. S. 2009, ApJ, 699, 305
Harris, D. E., & Krawczynski, H. 2002, ApJ, 565, 244
Harris, D. E., Massaro, F., Cheung, C. C., et al. 2011, ApJ, 743, 177
Imazawa, R., Fukazawa, Y., & Takahashi, H. 2021, ApJ, 919, 110
Ishibashi, W., & Courvoisier, T. J. L. 2009, A&A, 495, 113
Krolik, J. H. 1998, ApJL, 498, L13
Li, Y.-R., Yuan, Y.-F., Wang, J.-M., Wang, J.-C., & Zhang, S. 2009, ApJ, 699, 513
Lin, J., Soon, W., & Baliunas, S. L. 2003, NewAR, 47, 53
Lin, R. P., & Schwartz, R. A. 1987, ApJ, 312, 462
Macchetto, F., Marconi, A., Axon, D. J., et al. 1997, ApJ, 489, 579
MAGIC Collaboration, Acciari, V. A., Ansoldi, S., et al. 2020, MNRAS, 492, 5354
McKinney, J. C., Tchekhovskoy, A., & Blandford, R. D. 2012, MNRAS, 423, 3083
Narayan, R., & Yi, I. 1995, ApJ, 452, 710
Plucinsky, P. P., Bogdan, A., Marshall, H. L., & Tice, N. W. 2018, Proc. SPIE, 10699, 106996B
Strubbe, L. E., & Quataert, E. 2009, MNRAS, 400, 2070
Wang, J.-M., Cheng, C., & Li, Y.-R. 2012, ApJ, 748, 147
Wilson, A. S., & Yang, Y. 2002, ApJ, 568, 133
Xiang, F., & Cheng, C. 2020, RAA, 20, 101
Xie, F.-G., & Zdziarski, A. A. 2019, ApJ, 887, 167
Yang, S., Yan, D., Dai, B., et al. 2019, MNRAS, 489, 2685
Yuan, F., Lin, J., Wu, K., & Ho, L. C. 2009, MNRAS, 395, 2183
Yuan, F., & Narayan, R. 2014, ARA&A, 52, 529
Yuan, F., Taam, R. E., Misra, R., Wu, X.-B., & Xue, Y. 2007, ApJ, 658, 282